



HAL
open science

Regularized Tensor Representative Coefficient Model for Hyperspectral Target Detection

Wenting Shang, Mohamad Jouni, Zebin Wu, Yang Xu, Mauro Dalla Mura,
Zhihui Wei

► **To cite this version:**

Wenting Shang, Mohamad Jouni, Zebin Wu, Yang Xu, Mauro Dalla Mura, et al.. Regularized Tensor Representative Coefficient Model for Hyperspectral Target Detection. *IEEE Geoscience and Remote Sensing Letters*, 2023, pp.1-1. 10.1109/lgrs.2023.3255905 . hal-03806916

HAL Id: hal-03806916

<https://hal.science/hal-03806916>

Submitted on 19 Oct 2022

HAL is a multi-disciplinary open access archive for the deposit and dissemination of scientific research documents, whether they are published or not. The documents may come from teaching and research institutions in France or abroad, or from public or private research centers.

L'archive ouverte pluridisciplinaire **HAL**, est destinée au dépôt et à la diffusion de documents scientifiques de niveau recherche, publiés ou non, émanant des établissements d'enseignement et de recherche français ou étrangers, des laboratoires publics ou privés.

Regularized Tensor Representative Coefficient Model for Hyperspectral Target Detection

Wenting Shang, Mohamad Jouni, *Member, IEEE*, Zebin Wu, *Senior Member, IEEE*, Yang Xu, *Member, IEEE*, Mauro Dalla Mura, *Senior Member, IEEE*, and Zihui Wei

Abstract—Target detection based on the representation of the hyperspectral image (HSI) has drawn the attention of researchers, given its powerful detection performance. The matrix-based approach inevitably loses spatial information and fails to explore the intrinsic multimodal structure of an HSI cube. In this paper, we propose a regularized tensor-based model without altering the data structure. The model assumes that an observed third-order HSI tensor is decomposed into the sum of a Total Variation-regularized Low-rank background tensor and a Sparse (TVLrS) target tensor. The two tensors are then represented as the mode-3 product of a third-order tensor called the Tensor Representation Coefficient (TRC), by a matrix representing the spectra dictionary. The model is coined as *TVLrS-TRC*. Since the construction of a pure dictionary is essential for the background extraction, here, the background dictionary atoms are selected by the kernel spectral angle mapper (KSAM), while the target dictionary construction is done through the target atoms prior information. The tensor nuclear norm (TNN) is utilized to characterize the low rankness of the TRC subspaces, the TV norm is performed on each frontal slice of the TRC to encode its spatial smoothness, and the sparsity of the target TRC is characterized by the ℓ_1 -norm. Extensive experiments on two real hyperspectral data sets demonstrate the advantage of the proposed detector in comparison with several conventional and state-of-the-art target detectors.

Index Terms—Hyperspectral target detection, tensor decomposition, tensor representation coefficient, tensor nuclear norm, kernel spectral angle mapper

I. INTRODUCTION

WITH intrinsic high spectral resolution and recently enhanced spatial resolution; hyperspectral imaging has been providing a powerful technology in depicting and differentiating a variation of materials of targets. In particular, hyperspectral imagery has become an advanced technique for earth observation-related applications, such as safety and security [1], environmental protection [2], precision agriculture [3], and medical science [4]. Among various applications, target

detection (TD) has drawn increasing attention from researchers [5].

TD is a supervised binary classification problem that aims to label each pixel as a target or background. Over the past century, there has been a dramatic advancement in TD methods. The spectral angle mapper (SAM) [6] is a straightforward detection algorithm that measures the spectral angle between the spectrum of each pixel and the given prior spectral signature of the target. The statistics based methods, such as the adaptive coherence/cosine estimator (ACE) [7], and matched subspace detector (MSD) [8], have been extensively applied in TD. The constrained energy minimization (CEM) [9] detection minimizes the total output power while constraining the target signature by a specific gain. Considering the nonlinear problem, the kernel based TD methods, including kernel spectral angle mapper (KSAM) [10], kernel adaptive subspace detector (KASD) [11], are applied to TD for mapping the data into a high-dimensional feature space. Nevertheless, the above mentioned methods need to assume background and target follow a specific distribution.

The sparse representation detection (SRD) algorithms belong to the representative-based model category, which assumes each pixel lies in a subspace that can be sparsely represented by the dictionary, having been successfully applied for TD [12], [13]. Considering the essential of the dictionary construction, Cheng *et al.* [12] proposed a decomposition model (DM) with background dictionary learning (BDL) for hyperspectral TD to recover a satisfactory background. After that, [13] assumes that each pixel can be linearly and sparsely represented by the prior target spectra and several background endmembers extracted from its neighborhood.

The aforementioned methods are based on matrix modeling, which would destroy the spatial or the spectral information since the HSI is essentially a cube of data; specifically, they make good use of the spectral information regardless of the spatial structure features. Thereafter, tensor analysis of HSIs has been considered to exploit this inner structure. Liu *et al.* [14] proposed Tensor Matched Subspace Detector (TMSD) for hyperspectral TD, which used a linear combination of target tensor blocks and background tensor blocks. TMSD has yet to assume the background and the target distribution. Afterward, a tensor SRD (TSRD) algorithm [15] took into account the spatial and spectral information jointly, extending atoms of the target and the background dictionaries into a third-order tensor without assuming distributions of the background and the target. Zhao *et al.* [16] proposed a hyperspectral TD algorithm based on Tucker decomposition dictionary learning,

This work was supported in part by the National Natural Science Foundation of China under Grant 61772274, Grant 62071233, and grant 61701238, in part by the Jiangsu Provincial Natural Science Foundation of China under grant BK20211570, grant BK20180018, and grant BK20170858, in part by the Fundamental Research Funds for the Central Universities under grant 30917015104, grant 30919011103, grant 30919011402, and grant 30921011209, and in part by the China Postdoctoral Science Foundation under grant 2017M611814. (*Corresponding author: Zebin Wu.*)

W. Shang, Y. Xu, Z. Wu and Z. Wei are with the School of Computer Science and Engineering, Nanjing University of Science and Technology, Nanjing 210094, China (e-mail: shangwt1011@gmail.com; xuyangth90@njust.edu.cn; wuzb@njust.edu.cn; gswei@njust.edu.cn).

M. Jouni and M. Dalla Mura are with Univ. Grenoble Alpes, CNRS, Grenoble INP*, GIPSA-Lab, 38000 Grenoble, France (*Institute of Engineering Univ. Grenoble Alpes). M. Dalla Mura is also with the Institut Universitaire de France (IUF). (e-mail: mohamad.jouni@gipsa-lab.fr; mauro.dalla-mura@gipsa-lab.fr)

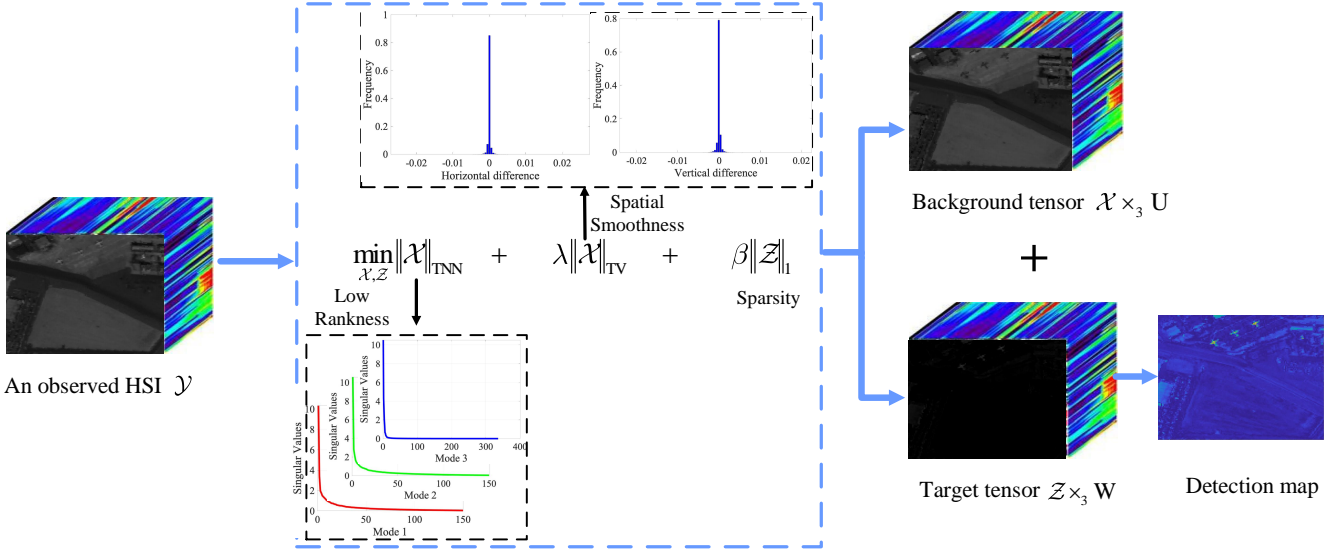


Fig. 1: The flowchart of the TVLrS-TRC for hyperspectral TD.

establishing a detection model based on sparse representation and collaborative representation. Finally, the above tensor-based methods ignored exploiting the physical characteristics of the representation coefficient, either the background or the target.

Given the concerns mentioned above, we propose a novel tensor-based hyperspectral TD method that exploits the physical characteristics of the TRCs for each of the target and background components of the observed HSI. Since a dictionary construction is essential for the recovery of both the background and target, we adopt KSAM for the background dictionary atoms selection, while the target atoms are chosen thanks to the prior information.

The rest of the paper is structured as follows. Section II introduces our proposed method. Section III provides the experimental evaluation and discussions. Finally, Section IV concludes this work.

II. PROBLEM FORMULATION

A. Tensor-based HSI Target Detection

Given an observed third-order HSI $\mathcal{Y} \in \mathbb{R}^{H \times W \times D}$, where H , W , and D represent the height, width, and number of the spectral bands respectively, we assume that \mathcal{Y} is the superposition of a background tensor $\mathcal{B} \in \mathbb{R}^{H \times W \times D}$ and a target one $\mathcal{E} \in \mathbb{R}^{H \times W \times D}$, and our aim is to accurately separate the target from the background such that:

$$\mathcal{Y} = \mathcal{B} + \mathcal{E}, \quad (1)$$

Furthermore, any third-order tensor can be linearly decomposed or represented as the mode-3 product of another third-order tensor by a matrix. \mathcal{B} and \mathcal{E} can then be represented as:

$$\mathcal{B} = \mathcal{X} \times_3 \mathbf{U}, \quad \mathcal{E} = \mathcal{Z} \times_3 \mathbf{W}, \quad (2)$$

where $\mathbf{U} \in \mathbb{R}^{D \times M}$ represents the background dictionary that need to be constructed, and $\mathbf{W} \in \mathbb{R}^{D \times N}$ is a prior target dictionary. Here, each column of both the \mathbf{U} and \mathbf{W} represents

the spectra of each pixel. $\mathcal{X} \in \mathbb{R}^{H \times W \times M}$ and $\mathcal{Z} \in \mathbb{R}^{H \times W \times N}$ represent the Tensor Representative Coefficients (TRCs) of the background and target terms respectively. Here, M and N represent the number of atoms of the background and the target respectively. In fact, expressions (1) and (2) mean that each tube-wise vector of observed third-order tensor HSI can be expressed as the sum of the linear combination of M atoms from the background spectral dictionary and N atoms from the target one:

$$\mathcal{Y} = \mathcal{X} \times_3 \mathbf{U} + \mathcal{Z} \times_3 \mathbf{W}. \quad (3)$$

As a better dictionary construction can provide a better background recovery, we use KSAM for the selection of the background dictionary atoms. Since TD is a supervised classification problem, we incorporate *a priori* target dictionary to the model.

B. TRC Prior Modeling

In addition to the dictionary construction, the exploitation of the structure of the TRC components is crucial for enhancing the performance as it has been pointed out that the TD accuracy depends greatly on the background modeling [17]. Specifically, the decompositions in eq.2 are not unique, as different factors could provide the same result after the mode-3 product. Thus there is the need to reduce this intrinsic ambiguity by considering some a priori information for constraining the space of possible solutions to only those that are compliant with the problem. Fig. 1 shows the plots of the singular values of the three modes (two spatial and one spectral) of the background TRC \mathcal{X} , which are observed to lie on low-rank subspaces. Thus, we deduce that \mathcal{X} enjoys a *low-rank* property. In addition, as depicted in Fig. 1, there exists a strong local *smoothness* structure on each frontal slice along the mode-3 direction of \mathcal{X} (i.e., on each spectral channel). Finally, since the target occupies a small proportion of the scene, we assume that its TRC \mathcal{Z} is *sparse*.

C. Proposed Model

Underlying the above prior modeling analysis for TD, in this paper, we propose a TV-regularized Low-rank and Sparse TRC-based (TVLrS-TRC) tensor decomposition for TD. Consequently, tensor nuclear norm (TNN) [17] is employed on the TRC to encode its low-rank property. The TNN of \mathcal{X} is the sum of singular values of all the frontal slices of $\widehat{\mathcal{X}}$, which is defined as $\|\mathcal{X}\|_{\text{TNN}} = \sum_{k=1}^M \|\widehat{\mathcal{X}}^{(k)}\|_*$. $\|\cdot\|_*$ is the matrix nuclear norm. Besides, total variation (TV) is introduced to promote the spatial piece-wise smoothness of \mathcal{X} . Sparsity with ℓ_1 -norm is imposed on \mathcal{Z} . The optimization problem of the proposed method is written as follows:

$$\begin{aligned} \min_{\mathcal{X}, \mathcal{Z}} \|\mathcal{X}\|_{\text{TNN}} + \lambda \|\mathcal{X}\|_{\text{TV}} + \beta \|\mathcal{Z}\|_1 \\ \text{s.t. } \mathcal{Y} = \mathcal{X} \times_3 \mathbf{U} + \mathcal{Z} \times_3 \mathbf{W}, \end{aligned} \quad (4)$$

where $\|\cdot\|_{\text{TNN}}$ is the low rank tensor nuclear norm, $\|\cdot\|_{\text{TV}}$ is TV norm on each channel image of \mathcal{X} , $\|\cdot\|_1$ is the ℓ_1 -norm.

The TV norm of the tensor \mathcal{X} is defined as:

$$\|\mathcal{X}\|_{\text{TV}} = \|\mathcal{H}\mathcal{X}\|_1 = \|\mathcal{H}_1\mathcal{X}\|_1 + \|\mathcal{H}_2\mathcal{X}\|_1, \quad (5)$$

let $\mathcal{X}_{i,j,k} |_{i \in \{1, \dots, H\}, j \in \{1, \dots, W\}, k \in \{1, \dots, M\}}$ indicate the intensity at the voxel (i, j, k) and $\mathcal{H}_1, \mathcal{H}_2$ be the two horizontal and vertical differential operators in the spatial domain. Then, we have:

$$\begin{cases} \mathcal{H}_1\mathcal{X}_{i,j,k} = \mathcal{X}_{i+1,j,k} - \mathcal{X}_{i,j,k} \\ \mathcal{H}_2\mathcal{X}_{i,j,k} = \mathcal{X}_{i,j+1,k} - \mathcal{X}_{i,j,k}. \end{cases} \quad (6)$$

The optimization problem in (4) can be solved by alternating direction method of multipliers (ADMM), in which auxiliary variables \mathcal{V}_1 , and \mathcal{V}_2 are introduced to separate the objective function, and transformed into the following equivalent formulation:

$$\begin{aligned} \min_{\mathcal{X}, \mathcal{Z}} \|\mathcal{X}\|_{\text{TNN}} + \lambda \|\mathcal{X}\|_{\text{TV}} + \beta \|\mathcal{Z}\|_1 \\ \text{s.t. } \mathcal{Y} = \mathcal{X} \times_3 \mathbf{U} + \mathcal{Z} \times_3 \mathbf{W}, \mathcal{V}_1 = \mathcal{X}, \mathcal{V}_2 = \mathcal{H}\mathcal{V}_1. \end{aligned} \quad (7)$$

The optimization problem in (4) by augmented Lagrangian function can be written as

$$\begin{aligned} \mathcal{L}(\mathcal{X}, \mathcal{V}_1, \mathcal{V}_2, \mathcal{Z}, \mathcal{D}_1, \mathcal{D}_2, \mathcal{D}_3, \mu) \\ = \|\mathcal{X}\|_{\text{TNN}} + \lambda \|\mathcal{V}_2\|_1 + \beta \|\mathcal{Z}\|_1 + \mu/2 \|\mathcal{V}_1 - \mathcal{X} - \mathcal{D}_1/\mu\|_F^2 + \mu/2 \\ \|\mathcal{V}_2 - \mathcal{H}\mathcal{V}_1 - \mathcal{D}_2/\mu\|_F^2 + \mu/2 \|\mathcal{Y} - \mathcal{X} \times_3 \mathbf{U} - \mathcal{Z} \times_3 \mathbf{W} - \mathcal{D}_3/\mu\|_F^2, \end{aligned} \quad (8)$$

1) Update \mathcal{X} :

$$\begin{aligned} \mathcal{X}^{(k+1)} = \arg \min_{\mathcal{X}} \|\mathcal{X}\|_{\text{TNN}} + \mu/2 \|\mathcal{V}_1^{(k)} - \mathcal{X}^{(k)} - \mathcal{D}_1^{(k)}/\mu\|_F^2 + 1/2 \|\mathcal{Y} \\ - \mathcal{X}^{(k)} \times_3 \mathbf{U} - \mathcal{Z}^{(k)} \times_3 \mathbf{W}\|_F^2 \\ = \arg \min_{\mathcal{X}} \|\mathcal{X}\|_{\text{TNN}} + \mu\eta_1/2 \|\mathcal{X} - \mathcal{X}^{(k)} + [(\mathcal{Y} - \mathcal{X}^{(k)} \times_3 \mathbf{U} - \mathcal{Z}^{(k)} \\ \times_3 \mathbf{W} - \mathcal{D}_3^{(k)}/\mu) \times_3 \mathbf{U}^T + (\mathcal{V}_1^{(k)} - \mathcal{X}^{(k)} - \mathcal{D}_1^{(k)})]/\eta_1\|_F^2, \end{aligned} \quad (9)$$

where $\eta_1 = \|\mathbf{U}\|_2^2$, and (9) has a closed-form solution by adopting the t-SVT operator [18].

TABLE I: AUC OF EACH COMPETITOR ON THE HYDICE DATA SET

Method	$AUC_{(P_D, P_F)}$	$AUC_{(P_D, \tau)}$	$AUC_{(P_F, \tau)}$
ACE	0.9631	0.2249	0.0048
CEM	0.9742	0.4531	0.1126
CSCR	0.9987	0.7371	0.3487
DM-BDL	0.9990	0.5960	0.0641
TVLrS-TRC	0.9997	0.5319	0.0260

TABLE II: AUC OF EACH COMPETITOR ON THE AVIRIS DATA SET

Method	$AUC_{(P_D, P_F)}$	$AUC_{(P_D, \tau)}$	$AUC_{(P_F, \tau)}$
ACE	0.9867	0.1660	0.0056
CEM	0.9727	0.0876	0.0215
CSCR	0.9918	0.6521	0.5594
DM-BDL	0.9943	0.5752	0.0619
TVLrS-TRC	0.9978	0.6119	0.1400

2) Update \mathcal{V}_1 :

$$\begin{aligned} \mathcal{V}_1^{(k+1)} = \arg \min_{\mathcal{V}_1} \|\mathcal{V}_1^{(k)} - \mathcal{X}^{(k+1)} - \mathcal{D}_1^{(k)}/\mu\|_F^2 + \|\mathcal{V}_2^{(k)} - \mathcal{H}\mathcal{V}_1^{(k)} \\ - \mathcal{D}_2^{(k)}/\mu\|_F^2, \end{aligned} \quad (10)$$

which can be optimized by the following linear system:

$$\mathcal{V}_1^{(k+1)} = (\mathbf{I} + \mathcal{H}^* \mathcal{H})^{-1} [\mathcal{X}^{(k+1)} + \mathcal{D}_1^{(k)}/\mu + \mathcal{H}^* (\mathcal{V}_2^{(k)} - \mathcal{D}_2^{(k)}/\mu)]. \quad (11)$$

3) Update \mathcal{V}_2 :

$$\mathcal{V}_2^{(k+1)} = \arg \min_{\mathcal{V}_2} \lambda \|\mathcal{V}_2^{(k)}\|_1 + \mu/2 \|\mathcal{V}_2^{(k)} - \mathcal{H}\mathcal{V}_1^{(k+1)} - \mathcal{D}_2^{(k)}/\mu\|_F^2, \quad (12)$$

which can be solved by the soft-thresholding function.

4) Update \mathcal{Z} :

$$\begin{aligned} \mathcal{Z}^{(k+1)} = \arg \min_{\mathcal{Z}} \beta \|\mathcal{Z}^{(k)}\|_1 + \|\mathcal{Y} - \mathcal{X}^{(k+1)} \times_3 \mathbf{U} - \mathcal{Z}^{(k)} \times_3 \\ \mathbf{W} - \mathcal{D}_3^{(k)}/\mu\|_F^2, \end{aligned} \quad (13)$$

combining (9) with (12), the sub-problem can be solved as follows,

$$\begin{aligned} \text{soft}(\beta/(\mu\eta_2), \\ \mathcal{Z}^{(k)} + (\mathcal{Y} - \mathcal{X}^{(k+1)} \times_3 \mathbf{U} - \mathcal{Z}^{(k)} \times_3 \mathbf{W} - \mathcal{D}_3^{(k)}/\mu) \times_3 \mathbf{W}^T / \eta_2), \end{aligned} \quad (14)$$

where $\eta_2 = \|\mathbf{W}\|_2^2$.

5) Update \mathcal{D}_1 :

$$\mathcal{D}_1^{(k+1)} = \mathcal{D}_1^{(k)} + \mu(\mathcal{X}^{(k+1)} - \mathcal{V}_1^{(k+1)}). \quad (15)$$

6) Update \mathcal{D}_2 :

$$\mathcal{D}_2^{(k+1)} = \mathcal{D}_2^{(k)} + \mu(\mathcal{H}\mathcal{V}_1^{(k+1)} - \mathcal{V}_2^{(k+1)}). \quad (16)$$

7) Update \mathcal{D}_3 :

$$\mathcal{D}_3^{(k+1)} = \mathcal{D}_3^{(k)} + \mu(\mathcal{X}^{(k+1)} \times_3 \mathbf{U} + \mathcal{Z}^{(k+1)} \times_3 \mathbf{W} - \mathcal{Y}). \quad (17)$$

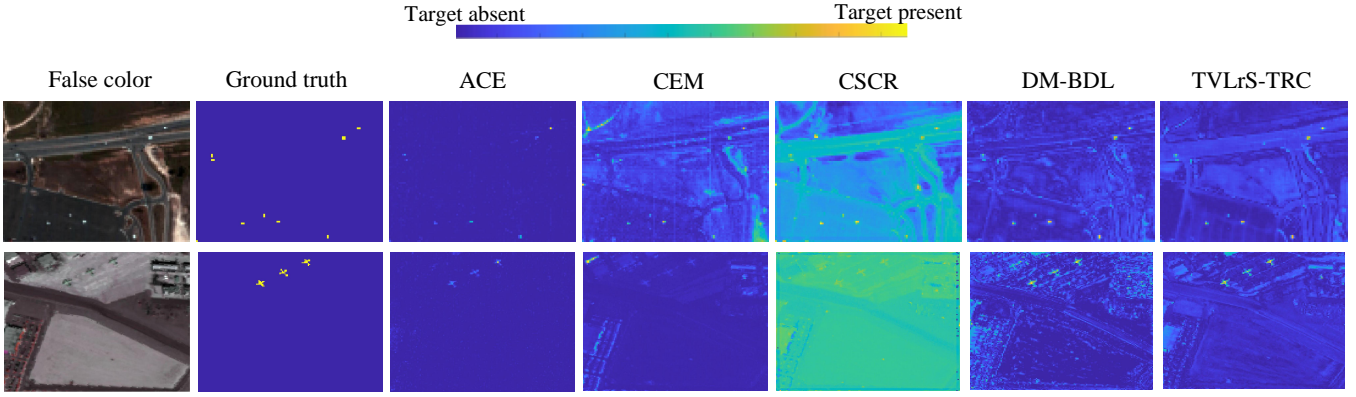


Fig. 2: 2-D plots obtained by different detectors on the HYDICE and AVIRIS datasets for TD.

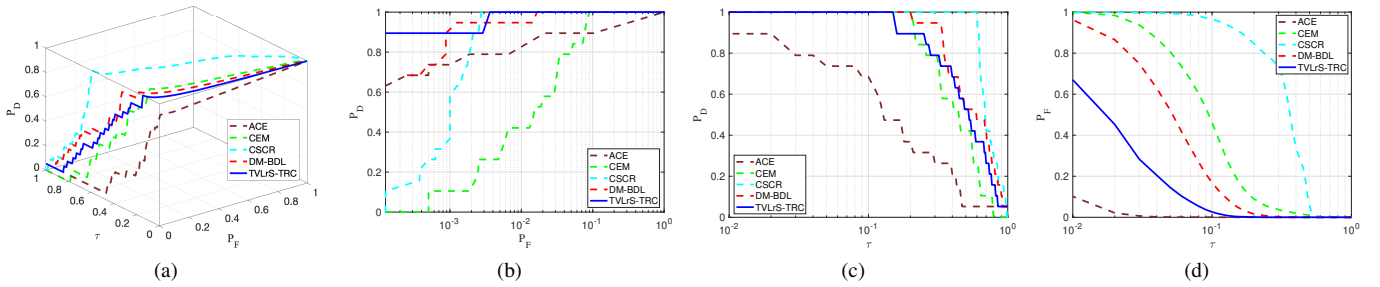


Fig. 3: The ROC curves of different comparing methods on HYDICE dataset. (Left to right) (a) 3D-ROC curve of (P_D, P_F, τ) , (b) 2D-ROC curve of (P_D, P_F) , (c) 2D-ROC curve of (P_D, τ) , and (d) 2D-ROC curve of (P_F, τ) .

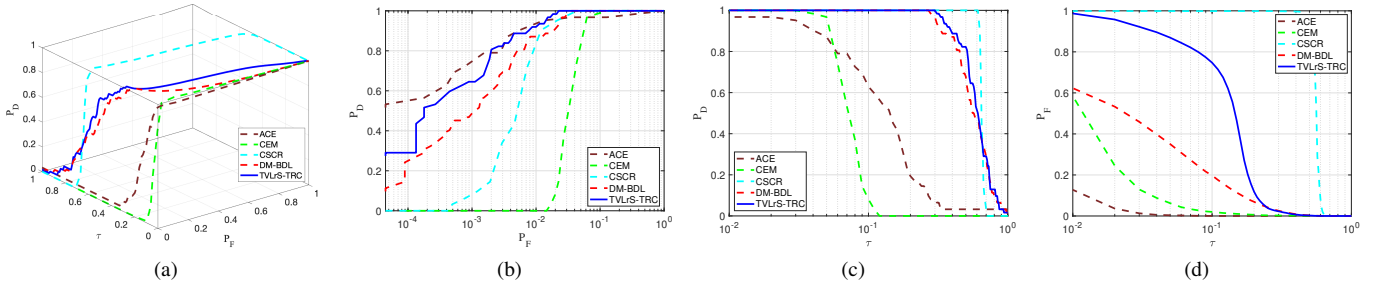


Fig. 4: The ROC curves of different comparing methods on AVIRIS dataset. (Left to right) (a) 3D-ROC curve of (P_D, P_F, τ) , (b) 2D-ROC curve of (P_D, P_F) , (c) 2D-ROC curve of (P_D, τ) , and (d) 2D-ROC curve of (P_F, τ) .

8) Update penalty scalar μ :

$$\mu = \min(\mu_{max}, \rho\mu). \quad (18)$$

III. EXPERIMENTAL RESULTS

In this section, we evaluate the performance of the proposed method by using two real hyperspectral images HYDICE and AVIRIS. The first real dataset was collected by the hyperspectral digital imagery collection experiment (HYDICE) sensor over an urban area. The whole image contains 307×307 pixels, and a region of interest with 80×100 pixels (rows 1–80 and columns 188–287) is cropped, preserving 162 bands after discarding the low SNR and water absorption bands to perform TD. The second dataset is obtained by Airborne Visible/Infrared

Imaging Spectrometer (AVIRIS) over San Diego, California, USA. There are left 191 spectral bands after removing the low signal-to-noise ratio (SNR) and water-absorption bands, and the upper left corner area is selected with the size of 150×150 .

In order to demonstrate the performance of the proposed method, we choose four methods as the base of comparison including the ACE [7], CEM [9], CSCR [12], and DM-BDL [19], carried on the two datasets for TD. To evaluate the performance of the detectors, we use 3-D Receiver Operating Characteristic (3D-ROC) (P_D, P_F, τ) [20] and three 2D-ROC curves such that:

- (P_D, P_F) assesses the overall detection performance
- (P_D, τ) evaluates the target preservation
- (P_F, τ) evaluates the background suppression

As such, the performance tends to be favorable as $(P_D, P_F) \rightarrow 1$,

$(P_D, \tau) \rightarrow 1$, and $(P_F, \tau) \rightarrow 0$. It is desired that the curves of (P_D, P_F) , (P_D, τ) , and (P_F, τ) are close to the upper left, upper right, and lower left corners of the coordinate axis, respectively.

For the HYDICE dataset, we select two atoms from the target atoms set to construct the target dictionary. The best performance is achieved when the parameters of the HYDICE dataset are set to $\lambda = 0.06$ and $\beta = 0.03$. In Table I, the (P_D, P_F) value of TVLrS-TRC is the highest, meanwhile, the target in the Fig. 3 are clearly preserved, and the ROC curve of the proposed TVLrS-TRC is closest to the upper left corner as shown in Fig. 3 (b). The (P_F, τ) of ACE is the lowest indicating its efficiency in background suppression, the corresponding scene also proves in Fig. 2. However, we can observe that both the (P_D, P_F) , and (P_D, τ) values of ACE are much lower than the other comparison methods, especially the proposed TVLrS-TRC method, referring to a low TD performance. According to the evaluation measure of 3D ROC, we can comprehensively evaluate that the tensor-based method TVLrS-TRC exploits better the inner physical meaning of both background and target TRCs, and achieves an excellent performance.

For the AVIRIS dataset, we select three atoms from the target atoms set to construct the target dictionary. The best performance is achieved when we set $\alpha = 0.5$, $\beta = 0.02$. TABLE II and Fig. 4 are from the quantitative and qualitative views to prove that the proposed TVLrS-TRC performs an excellent TD result. Specifically, Fig. 4(b) shows the 2D plot of the TVLrS-TRC method located at the bottom left corner. Its (P_D, P_F) is the highest, which further confirms its efficiency. As observed in TABLE II and Fig. 4 (d), both ACE and CEM methods are efficient in suppressing the background, but both methods perform inferior in terms of target preservation as shown in II and Fig. 4 (c). Finally, compared to the competitive DM-BDL method, our proposed method provides a better TD accuracy and target preservation as seen from the highest AUC value of (P_D, P_F) with a lower (P_D, τ) value.

In summary, we adopt the 3D ROC from a quantitative and a qualitative perspective in order to evaluate the performance of the proposed TVLrS-TRC model. From one side, the TVLrS-TRC is a tensor-based method with well preserved spatial and spectral information. From another side, a reasonable characterization of both background and target TRCs further enhances the accuracy of the TD result.

IV. CONCLUSION

In this letter, we proposed a tensor-based TD method named TVLrS-TRC. The observed third-order tensor HSI can be decomposed into the background tensor and the target tensor, each of them can be represented by the mode-3 product of TRC and the spectra dictionary matrix. As observed that all the three unfolded modes of background TRC with a low-rank property; thus, TNN is adopted to encode its low rankness. Moreover, TV is utilized to promote the spatial smoothness of each frontal slice of the TRC. Due to the target of interest occupying a few pixels in the whole scene, the ℓ_1 -norm is utilized for encoding sparsity of TRC. The KSAM is utilized to select the dictionary atoms for constructing a purer background dictionary, while the target dictionary atoms are chosen depending on the target's

prior information. The experiments and analysis on two real data sets demonstrate that the proposed method is superior to the other comparison algorithms in terms of TD accuracy and background suppression.

REFERENCES

- [1] V. C. Coffey, "Hyperspectral imaging for safety and security," *Optics and Photonics News*, vol. 26, no. 10, pp. 26–33, 2015.
- [2] E. Honkavaara, H. Saari, J. Kaivosoja, I. Pölonen, T. Hakala, P. Litkey, J. Mäkyinen, and L. Pesonen, "Processing and assessment of spectrometric, stereoscopic imagery collected using a lightweight uav spectral camera for precision agriculture," *Remote Sensing*, vol. 5, no. 10, pp. 5006–5039, 2013.
- [3] P. K. Sathy, C. Pandey, Y. K. Sahu, and S. K. Behera, "Hyperspectral imagery applications for precision agriculture—a systemic survey," *Multimedia Tools and Applications*, pp. 1–34, 2021.
- [4] A. Kaul *et al.*, "Hyperspectral imaging and target detection algorithms: a review," *Multimedia Tools and Applications*, pp. 1–66, 2022.
- [5] C.-I. Chang, "Hyperspectral target detection: Hypothesis testing, signal-to-noise ratio, and spectral angle theories," *IEEE Transactions on Geoscience and Remote Sensing*, vol. 60, pp. 1–23, 2022.
- [6] F. A. Kruse, A. Lefkoff, J. Boardman, K. Heidebrecht, A. Shapiro, P. Barloon, and A. Goetz, "The spectral image processing system (sips)—interactive visualization and analysis of imaging spectrometer data," *Remote sensing of environment*, vol. 44, no. 2-3, pp. 145–163, 1993.
- [7] S. Kraut and L. L. Scharf, "The cfar adaptive subspace detector is a scale-invariant glrt," *IEEE Transactions on Signal Processing*, vol. 47, no. 9, pp. 2538–2541, 1999.
- [8] L. Scharf and B. Friedlander, "Matched subspace detectors," *IEEE Transactions on Signal Processing*, vol. 42, no. 8, pp. 2146–2157, 1994.
- [9] W. H. Farrand and J. C. Harsanyi, "Mapping the distribution of mine tailings in the coeur d'alene river valley, idaho, through the use of a constrained energy minimization technique," *Remote Sensing of Environment*, vol. 59, no. 1, pp. 64–76, 1997.
- [10] G. Camps-Valls, "Kernel spectral angle mapper," *Electronics letters*, vol. 52, no. 14, pp. 1218–1220, 2016.
- [11] H. Kwon and N. M. Nasrabadi, "Kernel adaptive subspace detector for hyperspectral imagery," *IEEE geoscience and remote sensing letters*, vol. 3, no. 2, pp. 271–275, 2006.
- [12] T. Cheng and B. Wang, "Decomposition model with background dictionary learning for hyperspectral target detection," *IEEE Journal of Selected Topics in Applied Earth Observations and Remote Sensing*, vol. 14, pp. 1872–1884, 2021.
- [13] Q. Ling, K. Li, Z. Li, Z. Lin, and J. Wang, "Hyperspectral detection and unmixing of subpixel target using iterative constrained sparse representation," *IEEE Journal of Selected Topics in Applied Earth Observations and Remote Sensing*, vol. 15, pp. 1049–1063, 2022.
- [14] Y. Liu, G. Gao, and Y. Gu, "Tensor matched subspace detector for hyperspectral target detection," *IEEE Transactions on Geoscience and Remote Sensing*, vol. 55, no. 4, pp. 1967–1974, 2017.
- [15] Z. Chen and B. Wang, "Hyperspectral target detection based on tensor sparse representation," *IEEE Geoscience and Remote Sensing Letters*, vol. 16, no. 10, pp. 1605–1609, 2019.
- [16] C. Zhao, M. Wang, N. Su, and S. Feng, "Dictionary learning hyperspectral target detection algorithm based on tucker tensor decomposition," in *IGARSS 2020-2020 IEEE International Geoscience and Remote Sensing Symposium*. IEEE, 2020, pp. 1763–1766.
- [17] L. Deng, D. Xu, G. Xu, and H. Zhu, "A generalized low-rank double-tensor nuclear norm completion framework for infrared small target detection," *IEEE Transactions on Aerospace and Electronic Systems*, 2022.
- [18] Y. Xu, R. Hao, W. Yin, and Z. Su, "Parallel matrix factorization for low-rank tensor completion," *arXiv preprint arXiv:1312.1254*, 2013.
- [19] W. Li, Q. Du, and B. Zhang, "Combined sparse and collaborative representation for hyperspectral target detection," *Pattern Recognition*, 2015.
- [20] C.-I. Chang, "Multiparameter receiver operating characteristic analysis for signal detection and classification," *IEEE Sensors Journal*, vol. 10, no. 3, pp. 423–442, 2010.